h_{fg} = enthalpy of vaporization, B.t.u./lb.-m
$h_F°$ = stagnation enthalpy of mixture entering test section, B.t.u./lb.-m
J = mechanical equivalent of heat
P = pressure, lb./sq.in.abs.
P_c = critical pressure, lb./sq.in.abs.
P_{th} = pressure at test section exit, lb./sq.in.abs.
P_b = expansion chamber pressure, lb./sq.in.abs.
V = specific volume, cu.ft./lb.-m
V_g = vapor specific volume, cu.ft./lb.-m
X = vapor quality, %
X' = weight fraction steam
X_{TH} = vapor quality at exit based on an energy balance with the homogeneous model [Equation (5)]

LITERATURE CITED

1. Agostinelli, A., and V. Saleman, *Trans. Am. Soc. Mech. Engrs.*, **80**, 1138-1142 (1958).
2. Allen, W. F., Jr., *ibid.*, **73**, 257-265 (1951).
3. Allen, C. M., and L. J. Hooper, *ibid.*, **54**, Hyd-54-1 (1932).
4. Bailey, J. F., *ibid.*, **73**, 1109-1116 (1951).
5. Benjamin, M. W., and J. C. Miller, *ibid.*, **64**, 657-669 (1942).
6. Bottomley, W. F., *Trans. North East Coast Inst. Engrs. and Shipbuilders*, **53**, 65-100 (1937).
7. Brooks, Burton, Personal communication, Chemithon Corp., Seattle, Washington.
8. Burnell, J. G., *Engineering*, **164**, 572-576 (1947).
9. Cruz, A. J. R., M.S. thesis, University of Minnesota, Minneapolis, Minnesota (1953).
10. Faletti, D. W., Ph.D. thesis, University of Washington, Seattle, Washington (1959).
11. Fauske, H., and H. S. Isbin, *TID-11061* (1961).
12. Firey, J. C., Personal communication, University of Washington, Seattle, Washington.
13. Hoogendoorn, G. J., *Chem. Eng. Sci.*, **9**, 205 (Feb., 1959).
14. Hoopes, J. W., *A.I.Ch.E. Journal*, **3**, 268-275 (1957).
15. Isbin, H. S., J. E. Moy, and A. J. R. Cruz, *ibid.*, pp. 361-365.
16. Keenan, J. H., and F. G. Keyes, Wiley, New York (1936).
17. Lining, D. L., *Proc. Inst. Mech. Engrs.*, **1B**, 64-75 (1952-53).
18. Mellanby, A. L., and W. Kerr, *Proc. Inst. Mech. Engrs.*, **2**, Part 2, pp. 844-883 (1922).
19. Moy, J. E., M.S. thesis, University of Minnesota, Minneapolis, Minnesota (1955).
20. Rettaliatta, J. T., *Trans. Am. Soc. Mech. Engrs.*, **58**, 599 (1936).
21. Ryley, D. J., 1 and 11, *Engineer 193*, 332033, 363-365 (1952).
22. Schwartz, A. M., and J. W. Perry, "Surface Active Agents," Vol. 1, pp. 286-288, Interscience, New York (1949).
23. Silver, R. S., and J. A. Mitchell, *Trans. North East Coast Inst. Engrs. and Shipbuilders*, **62**, 51-72, Disc. 15-30 (1945-46).
24. Silver, R. S., *Proc. Roy. Soc. (London)*, **A194**, 464-480 (1948).
25. Stodola, A., "Steam and Gas Turbines," p. 108-129, McGraw-Hill, New York (1927).
26. Stuart, D. O., and G. Murphy, *Am. Soc. Mech. Engrs. Paper No. 58-A-112* (Nov. 30-Dec. 5, 1958).
27. Stuart, M. C., and D. R. Yarnall, *Trans. Am. Soc. Mech. Engrs*, **66**, 387-395 (1955).
28. Yellott, J. J., *ibid.*, **56**, 411-430 (1934).
29. Zaloudek, F. R., *HW-68934*, Hanford Atomics Works (1961).

Manuscript received May 1, 1962; revision received August 24, 1962; paper accepted August 29, 1962.

A Study of Carry-Under Phenomena in Vapor Liquid Separation

MICHAEL PETRICK

Argonne National Laboratory, Argonne, Illinois

In systems where the circulating coolant is boiled, it becomes increasingly difficult to achieve effective primary separation of the phases as the systems volumetric capacity decreases and power density increases. When it is desired to effect this separation by purely natural means (gravity), the problem becomes acute. It is virtually impossible to effect a complete separation of the phases without the use of mechanical devices. A certain fraction of the vapor phase will be entrained in the downcomer with the recirculating liquid phase. The fraction of the vapor phase that is entrained in the downcomer is generally referred to as the *percent carry under*.

In boiling systems where the fluid flow is derived by means of natural convection, the carry-under problem can become especially crucial. This stems from the fact that the recirculation flow rates are a function of the density difference existing between the upcomer (riser) and downcomer segments of the system. Should substantial quantities of vapor be entrained by the circulating fluid in the downcomer, the performance of the system could suffer significantly. Forced circulation systems could also be adversely affected, since excessive carry under into the suction lines could lead to cavitation problems.

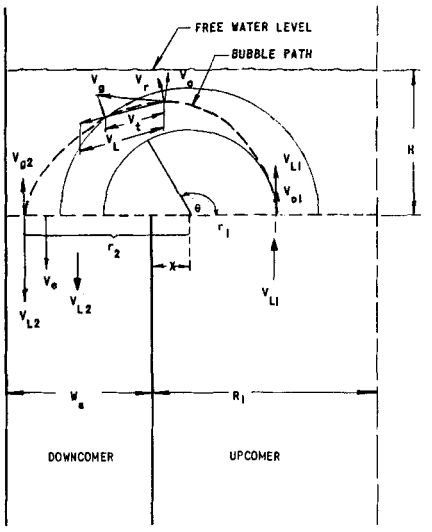

Fig. 1. Bubble trajectory in the separation plenum.

A schematic of a typical plenum where the separation process takes place is shown in Figure 1. The two-phase mixture enters the plenum through an upcomer and the recirculating coolant leaves the plenum through the downcomer. The separation of the vapor phase from the liquid phase must therefore occur by means of buoyant and hydrodynamic forces in the time interval between entrance and discharge of the coolant into the plenum. The average time interval can

Work performed under the auspices of the U.S. Atomic Energy Commission.

be relatively long or short and is determined primarily by the systems physical dimensions and volumetric flow of the vapor and liquid phases. There is virtually no information available which can be used for estimating the amount of carry under that would be obtained in a given system for varying operating conditions. As a result an analytical and experimental study of the carry-under problem was undertaken to establish both quantitatively and qualitatively the effect of pertinent parameters. The experimental phase of the problem was carried out on an atmospheric air-water loop and on a high-pressure steam-water loop. The air water studies were primarily aimed at establishing the pertinent parameters that affect the magnitude of carry under occurring. The purpose of the steam-water test was to determine the pressure effect on carry under.

THEORETICAL ANALYSES

Consider a typical plenum, as depicted in Figure 1, where the vapor liquid separation occurs. It is readily apparent that the amount of vapor phase entrainment that occurs is sensitive to the liquid phase flow path. As a result the first step in the analysis was a study of the fluid streamlines in a plenum. The analysis was made on a pseudo ideal two-dimensional system, whereas the plenum is, in fact, an axisymmetrical three-dimensional geometry. However the results were thought to be indicative of the true fluid streamlines. The fluid streamlines were determined by an electrical potential analogue. Basically the method consisted of determining the equipotential lines on Teledeltos paper (uniform resistivity paper).

Figure 2 shows the fluid streamlines that were determined for a plenum where the area ratio between the downcomer and riser was 2/1 and the true interface heights were $H = R/4$, $H = R$, $H = 2R$, and $H \to \infty$. As can be seen there is very little change in the flow pattern beyond an interface height of $H = 2R$. This is typical for any A_D/A_R ratio. Also the streamlines indicate that the liquid flowing out of the riser into the downcomer follow approximately circular paths. For the case where $H \geq 2R$ the radius of the circular streamlines can be approximated by the following relationship:

$$\bar{r} = \frac{f(R+W)}{2} \qquad (1)$$

The center of the circle would then be located at a distance x from the riser wall, where

$$x = \frac{f(R-W)}{2} \qquad (2)$$

The velocity of the water as it flows from the riser to the downcomer was assumed to vary in accordance with

$$V_L = \frac{V_{L,1} - V_{L,2}}{2}\cos\theta + \frac{V_{L,1} + V_{L,2}}{2} \qquad (3)$$

which is based on the boundary conditions when

$\theta = 0$, $V_L = V_{L,1}$ (water velocity in the riser)

$\theta = \frac{\pi}{2}$, $V_L = \frac{V_{L,1} + V_{L,2}}{2} = V_{L,3}$ (average cross-flow velocity)

$\theta = \pi$, $V_L = V_{L,2}$ (water velocity in the downcomer)

BUBBLE TRAJECTORY

Consider a bubble being entrained in a liquid that is following a circular path. Refer to Figure 1. The magnitude and direction of the absolute velocity of the bubble is given by

$$\vec{V}_g = \vec{V}_L + \vec{V}_o \qquad (4)$$

The absolute velocity of the bubble considered has the following radial and tangential components.

$$V_r = d\bar{r}/dt = V_o \sin\theta \qquad (5)$$

$$V_t = \bar{r}\, d\theta/dt = V_L + V_o \cos\theta \qquad (6)$$

Substituting Equation (3) into Equation (6) and combining with Equation (5) and simplifying one gets

$$\frac{\bar{r}}{\bar{r}_1} = \left(\frac{V_{L,1} + V_o}{(V_{L,1} - V_{L,2} + 2V_o\cos\theta)/2 + V_{L,3}}\right)^{2V_o/(2V_o + V_{L,1} - V_{L,2})} \qquad (7)$$

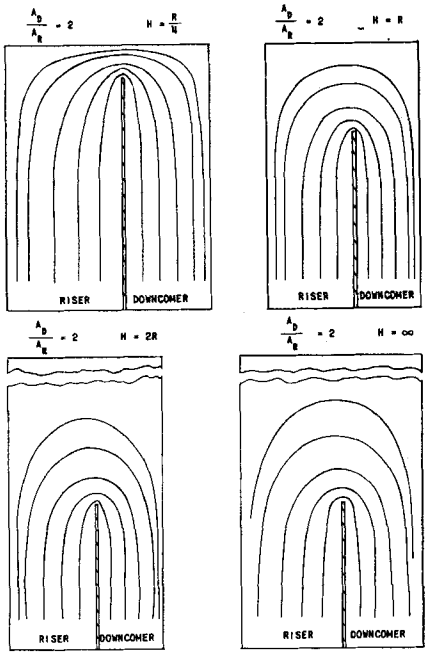

Fig. 2. Fluid streamlines in the separation plenum.

ENTRAINMENT CONDITIONS

Suppose a bubble following the above described motion completed a 180 deg. rotation and had a velocity $V_{g,2} = V_{L,2} - V_o$ at the section $\theta = \pi$. If $V_{L,2} > V_o$, the bubble will be entrained with the velocity $V_{g,2} = V_{L,2} - V_o$. If $V_{L,2} < V_o$, the bubble will rise with a velocity $V_{g,2} = V_o - V_{L,2}$. Consequently for entrainment one must have $V_o < V_{L,2}$. From a force balance on a bubble the condition becomes

$$\sqrt{\frac{4(\rho_L - \rho_g)g\,d_c}{3\,\rho_L\,C}} < V_{L,2} \qquad (8)$$

or

$$d_c < \frac{3\,C\,\rho_L}{4g(\rho_L - \rho_g)} V^2_{L,2}$$

A second condition of entrainment is that the radius of the circular trajectory that the bubble follows, as given by Equation (7), must fall within the downcomer annulus (see Figure 1). Therefore

$$\bar{r}_2 = \frac{f(R-W)}{2} + W \qquad (9)$$

Substituting Equation (1) into Equation (7) with $\theta = \pi$ one gets

$$\bar{r}_2 = \frac{f(W+R)}{2}\left[\frac{V_{L,1} + V_o}{V_{L,2} - V_o}\right]^{2V_o/(2V_o + V_{L,1} - V_{L,2})} \qquad (10)$$

Equating (9) and (10) one obtains

$$\frac{f(W+R)}{2}\left[\frac{V_{L,1} + V_o}{V_{L,2} - V_o}\right]^{2V_o/(2V_o + V_{L,1} - V_{L,2})} = \frac{f(R-W)}{2} + W \qquad (11)$$

Equation (11) specifies the second entrainment condition. When $V_o = V_{L,2}$, Equation (11) implies $f = 0$. Therefore at the periphery of the riser the maximum diameter of the bubble that will be entrained is given by Equation (8). When $V_o = 0$, Equation (11) reduces to $f = 1$, which satisfies the condition that not even the smallest size bubble emerging from the

center of the riser can be carried under. Equation (11) thus establishes the relationship between the maximum critical bubble diameter through the bubble velocity V_o, which can be entrained, and the position from which the bubble starts its motion.

When one solves Equation (11) for f

$$f = \frac{2W[(V_{L,2} - V_o)/(V_{L,1} + V_o)]^a}{W[1 + (V_{L,2} - V_o)/(V_{L,1} + V_o)]^a + R[1 - (V_{L,2} - V_o)/(V_{L,1} + V_o)]^a} \quad (12)$$

where

$$a = \frac{2V_o}{2V_o + V_{L,1} - V_{L,2}}$$

Equation (12) can then be used in conjunction with the average bubble size and liquid velocities to calculate a pseudo area in the riser from which the carry under emanates. That is a point is reached when one progresses from the periphery of the riser to its center beyond which the average sized bubble will not be carried under since its trajectory exceeds the width of the annulus. The distance in from the riser edge where this occurs is

$$L_c = fR \quad (13)$$

The area of the riser from which carry under occurs is given by

$$A_c = \int_{R-fR}^{R} 2\pi r dr \quad (14)$$

$$A_c = \pi R^2 (2f - f^2) = \pi R^2 [1 - (1-f)^2] \quad (15)$$

Some credulity is lent to the concept of a specific area of the riser from which the major portion of the carry under occurs [as specified by Equation (15)] by photographs that were taken of a plenum during operation. The circular type of trajectories of the bubble are readily apparent allowing for distortion due to the circular section. Also, as one moves toward the center of the riser, the bubble trajectories become wider and wider, intercept the outer wall, and then become engulfed in the large turbulent eddies existing near the surface. The major portion of the gas phase carried under appears to emanate from the peripheral region of the riser. A behavior pattern of this type is predicted by Equation (15).

PREDICTION OF CARRY UNDER

All the bubbles having $d < d_c$ (the critical bubble diameter) in that region of the riser specified by Equation (15) will be entrained. If the water velocity $V_{L,2}$ at the inlet of the downcomer is known, the critical diameter can be found by using Equation (8) and the drag coefficient vs. the Reynolds number relationship given in Figure 3. This relationship evolved after a scrutiny of a large amount of data obtained from the literature (*1, 2, 3, 4, 5, 6, 7, 8*) on the bubble velocity vs. the bubble diameter. Since there are very large discrepancies between the various sets of data, the development of the relationship shown in Figure 3 was guided by the assumption that the gas bubbles behaved almost as solid spheres in the Reynolds number range of $10 < Re < 900$, and by Pavlushenko's data (*2*) for $Re > 1{,}000$.

The volume of bubbles in a unit volume of riser is α_R and the number of bubbles in this unit volume is

$$\frac{N}{\text{cu. ft.}} = \frac{\bar{\alpha}_R}{4/3\,\pi\,\chi^3} \quad (16)$$

Therefore the bubble flow out from the region of the riser producing the carry under is

$$F_1 = \frac{\alpha_R V_{g,1} A_c}{4/3\,\pi\,\chi_1^3} \quad (17)$$

Similarly the bubble flow in the downcomer is

$$F_2 = \frac{\alpha_D (V_{g,2})}{4/3\,\pi\,\chi_2^3} A_D \quad (18)$$

A bubble balance between downcomer and riser yields

$$\frac{\alpha_D (V_{g,2})}{4/3\,\pi\,\chi_2^3} \pi (R_2^2 - R_1^2) = \frac{V_{g,1}}{4/3\,\pi\,\chi_1^3} (\bar{\alpha}_R)(A_c)(F_B) \quad (19)$$

The factor F_B represents the fraction of the bubbles in the riser whose diameter is less than d_c and are thus susceptible to carry under. To obtain this factor one must have data on the bubble sizes and distribution in two-phase mixtures. A limited study was made to obtain such data on air-water systems. The bubble size and distributions were determined by photographic techniques. The distributions were fitted by a normalized Poissons' equation:

$$N_n(\chi) = P(b\chi)^c \exp(-b\chi) \quad (20)$$

The constants in the equation were derived from the data and were found to be functions of the liquid and gas mass velocities and void fraction. They are

$$c = 17.7 \times 10^3 \left(\frac{V_T^{1.5}}{G^2}\right) \quad (21)$$

$$b = \frac{15.34}{(1-\alpha)^3} \quad (22)$$

$$P = \frac{b}{\Gamma(c+1)} \quad (23)$$

The average bubble size was found to be primarily a function of the average true liquid velocity. A plot of the average bubble size vs. the true liquid velocity is given in Figure 4. The number of bubbles susceptible to entrainment is therefore given by

$$F_B = \frac{\int_o^{d_c/2} P(b\chi)^c \exp(-b\chi)\, d\chi}{\int_o^{\infty} P(b\chi)^c \exp(-b\chi)\, d\chi} \quad (24)$$

The gas velocities in the riser and downcomer $V_{g,1}$ and $V_{g,2}$ can be represented by the following relations:

$$V_{g,1} = V_{L,1} + V_o \quad (25)$$

$$V_{g,2} = V_{L,2} - V_o \quad (26)$$

The average bubble velocity is shown as a function of the bubble diameter in Figure 5. This relationship was developed by relating the average bubble size to the average gas phase velocity which was computed from the measured void volume fractions and mixture qualities. Solving Equation (19) for the downcomer void fraction one obtains

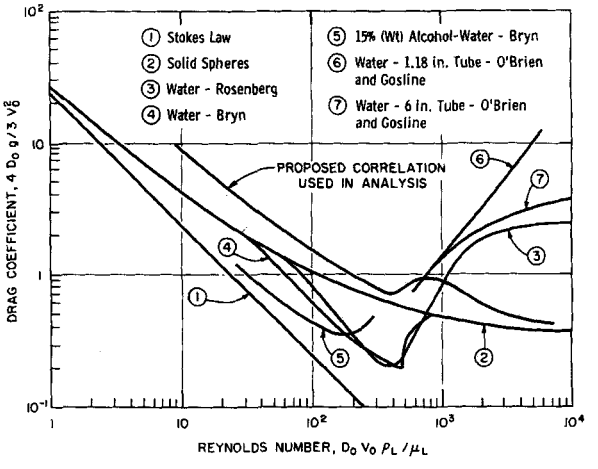

Fig. 3. Drag coefficient for bubbles rising in stagnant systems.

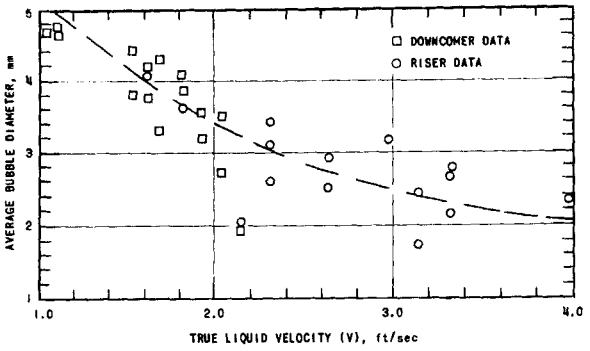

Fig. 4. Average bubble size vs. the true liquid velocity.

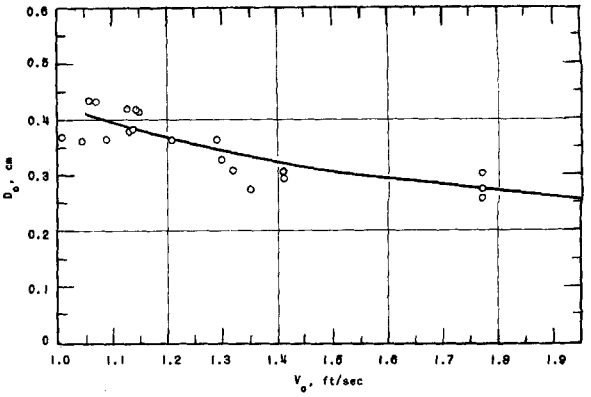

Fig. 5. Bubble velocity vs. bubble diameter in a flowing two-phase fluid.

$$\alpha_D = \left(\frac{\chi_2}{\chi_1}\right)^3 \frac{V_{L,1} + V_o}{V_{L,2} - V_o} (\bar{\alpha}_R) \left(\frac{A_c}{A_D}\right) (F_B) \quad (27)$$

Equation (27) states that the void fraction in the downcomer is a function of system geometry, bubble size in the riser and downcomer, the true liquid velocity in the riser and downcomer, and the mean void fraction in the riser. Equation (27) is essentially valid only when the interface height is much greater than the riser diameter.

Also

$$\frac{V_{L,1} + V_o}{V_{L,2} - V_o} = \frac{V_{g,1}}{V_{g,2}} = \frac{V_{L,1}}{1 - \alpha_R} \frac{(V_L/V_g)_R (1 - \alpha_D)}{(V_g/V_L)_D V_{L,2}} \quad (28)$$

and

$$\frac{\alpha}{1 - \alpha} = \frac{X}{(V_g/V_L)} \frac{\rho_L}{\rho_g} \quad (29)$$

When X is very small, Equation (27) becomes

$$\frac{X_D}{X_R} = \left(\frac{\chi_2}{\chi_1}\right)^3 \left(\frac{A_c}{A_R}\right) (F_B) \quad (30)$$

The quantity X_D/X_R is generally referred to as the *fractional carry under.*

A comparison was then made between Equation (30) and carry-under measurements taken from the air-water loop to check the validity of the analysis.

LABORATORY APPARATUS AND EXPERIMENTAL PROCEDURES

The carry-under studies were carried out on two laboratory loops, an atmospheric air-water system and a 2,000 lb./sq. in. steam-water system. Each of these systems and the experimental procedures associated with them are described below.

ATMOSPHERIC AIR-WATER LOOP

The air-water loop consists of a water circulation and air injection system, the mixing chamber, the separating plenum, the air-water separator, and associated instrumentation. The experimental apparatus is schematically illustrated in Figure 6.

Water is circulated through the system by means of two turbine types of pumps having a total combined capacity of approximately 300 gal./min. Regulation of the water flow rate was by means of a bypass system on the pump. The water flow rate was metered by means of a calibrated orifice.

The operating procedure was as follows. The desired air and water flow rates were set and the loop allowed to come to equilibrium. The temperature of the recirculating water was followed closely and maintained by adjustment of the cooling water flow rate. Equilibrium was established when the fluid temperature and the flow rate of the gas phase carried under, measured on the gas meter, approached constant values. The desired data were then recorded.

The mixture qualities in the riser and downcomer were obtained from the measured gas and liquid flow rate. The void fractions were calculated from differential pressure drops taken at strategic positions about the system. This procedure for determining the void fraction was corroborated by obtaining density traverses with a gamma source. The gamma attenuation techniques utilized have been described previously (9). Excellent agreement between the two methods was obtained.

Data were taken over the following parameter ranges on the air-water loop:

Riser void fraction	— α_R 0.1-0.50
Downcomer velocity	— $V_{D,1}$ ½-2½ ft./sec.
Riser quality	— $X_{R,1}$ 0.0002-0.003
Height of interface	— H 4-19 in.
Area of ratio between downcomer and riser	— A_D/A_R 1.70

HIGH-PRESSURE STEAM WATER LOOP

The high-pressure loop is schematically illustrated in Figure 7. It consists of a heated section where the two-

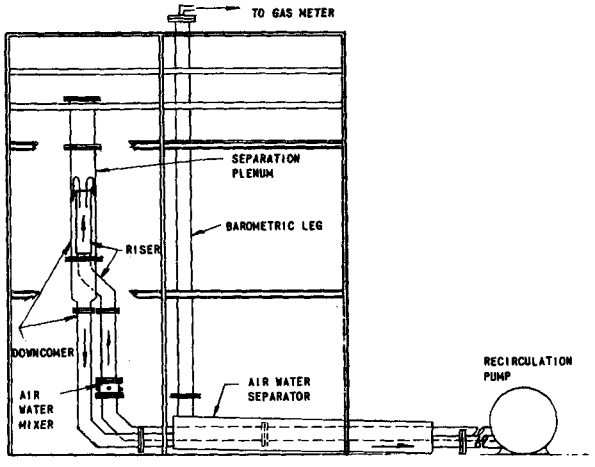

Fig. 6. Schematic of air-water loop.

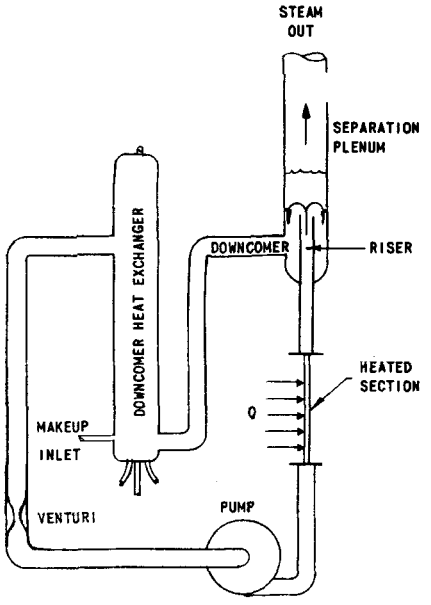

Fig. 7. Schematic of high-pressure loop.

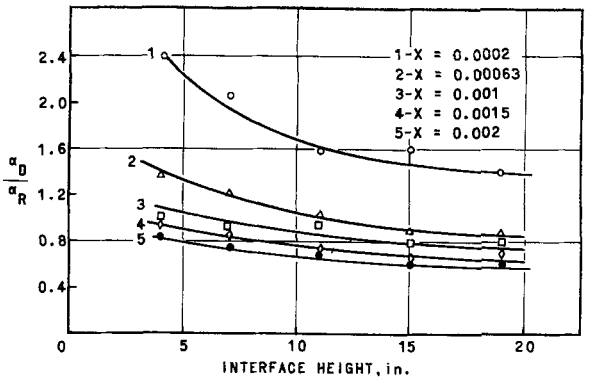

Fig. 9. Effect of height and quality of the volumetric entrainment ratio.

phase mixture is generated, a separation plenum similar to the one used on the air-water loop, a heat exchanger in the downcomer for measuring the quality of the mixture carried under, a make-up water system, and a steam condenser. Water is pumped from the make-up tank through the test section where it is boiled. The two-phase mixture then passes upward to the separation plenum where the separation of the phases occurs owing to gravity. The steam that is separated leaves the separation plenum, is metered, condensed, and returned to the make-up tank. The recirculation water and the steam carried under discharges through the annular downcomer to a heat exchanger where the mixture composition is determined by means of a heat balance. From the downcomer heat exchangers the fluid (now single phase) flows to the suction side of the recirculating pumps.

The operating procedure was as follows. The loop was gradually brought to saturation conditions at the desired pressure. When saturation was reached, the recirculating flow rate was adjusted to the desired value and the power was adjusted to yield the predetermined quality. The interface height was then adjusted slowly by creating an imbalance in the make-up water and steam discharge rate. The true interface height was determined by employing a gamma ray traverse. The interface was considered reached when a sharp increase in gamma intensity was observed. Concurrent with these operations the cooling water to the downcomer heat exchanger was adjusted continually to provide an adequate subcooling margin of ~ 5°F. The loop was then allowed to equilibrate and the data were recorded.

The quality of the two-phase mixture entering the separation plenum through the riser X_R was obtained by a simple heat balance on the test section. The quality of the two-phase mixture leaving the separation plenum through the downcomer X_D is calculated from a heat balance on the downcomer heat exchanger.

The steam volume fractions were again calculated from differential pressure drop measurements and corroborated by gamma traverse where possible.

The parameter ranges studied on the high-pressure loop were

Riser void fractions	— α_R 0.10-0.50
Pressures	— P 600, 1,000, 1,500 lb./sq.in.
Downcomer velocities	— $V_{D,1}$ 0.5-2.0 ft./sec.
Interface heights	— H 5-17 in.
Downcomer to riser area ratios	— A_D/A_R 1.6

COMPARISON OF AIR-WATER DATA WITH THE THEORETICAL ANALYSIS

The weight fraction ratio X_D/X_R was computed for thirty runs and compared with the experimentally measured values. The runs selected for comparison covered virtually the entire parameter range studied. The agreement between the measured and calculated values of

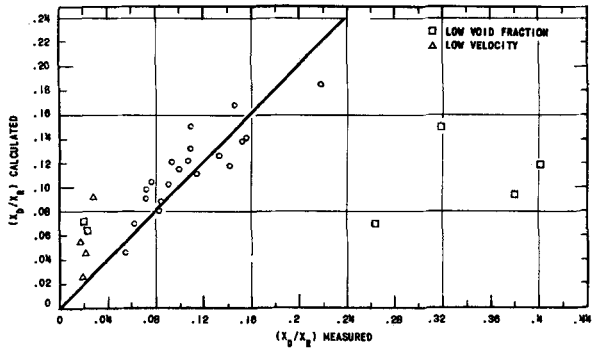

Fig. 8. Comparison of the measured and calculated weight fraction entrainment ratios.

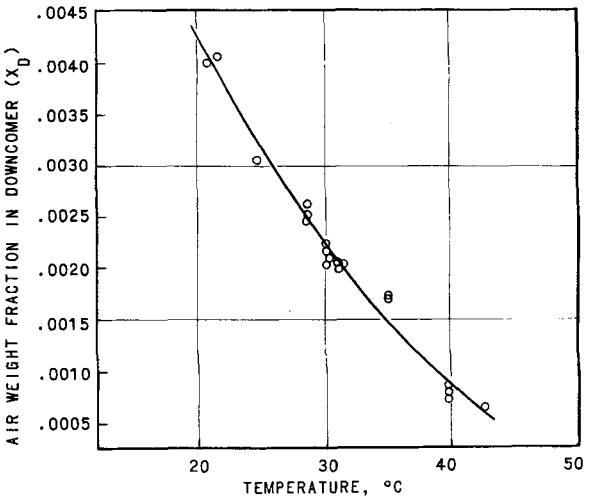

Fig. 10. Effect of temperature on carry under.

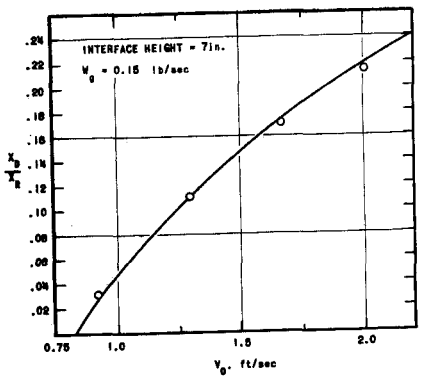

Fig. 11. Weight fraction carry under vs. the downcomer superficial liquid velocity.

the weight fraction ratio is good. A comparison is shown in Figure 8 by means of an error plot. The calculations showed that the carry under emanated from the extreme peripheral region of the riser. As mentioned previously, this was confirmed by visual observations and by trace photographs. The measured points that deviate widely from the calculated values are subject to question. The points that have a much lower calculated ratio, X_D/X_R, than measured are representative of very low riser void fractions (< 0.10). They are thought to be in error because of a distorted void distribution. It should be remembered that the air is introduced into the riser by means of a peripheral injection system. For a very low air rate it was observed that the air tended to remain at the periphery. Such a distribution could lead to excessive carry under. The data points which have much too high calculated values cover conditions where the downcomer velocity is low and is almost equal to the bubble bouyancy velocities. Under such conditions the slip ratios are extremely low and their accuracy is extremely sensitive to measured void fractions, which is then reflected in the velocity ratio $V_{g,1}/V_c$. It is felt that the measured void fractions in this range are in error, since it was observed that under these conditions some of the air escaped owing to coalescence after having been entrained. This leads to abnormally high void fractions and in turn to excessively low slip ratios and high velocity ratios. As a result the values of the calculated volumetric entrainment ratio α_D/α_R is extremely high.

From Equation (30) it can be seen that the percent carry under is governed primarily by the factor A_c which is the riser area from which the carry under emanates. The good agreement obtained between the predicted and measured values suggests that the proposed highly simplified carry-under model does describe the actual physical conditions existing in the plenum satisfactorily. However its validity is not completely established. Additional tests and data are needed on widely varying geometries and extended parameter ranges so that its effectiveness may be judged more certainly. Also more information on bubble size and distribution for various fluids and at various conditions of temperature and pressure are required before the analysis can be made more general and comprehensive.

DISCUSSION AND CORRELATION OF CARRY-UNDER DATA

Air-Water Data

The first series of air-water tests were run to study the effects of interface height on carry under. The liquid and gas flow rates were set and the interface height was then varied from $H/D = 4$ to $H/D = 0.75$. Typical results from these tests, in which the downcomer velocity was held constant, are shown in Figure 9. The volumetric carry-under ratios are plotted as a function of the interface height, and as can be seen a family of curves is obtained for the varying qualities. A similar family of curves is obtained when weight fraction carry-under ratio is plotted vs. the interface height. It is apparent that there is very little effect

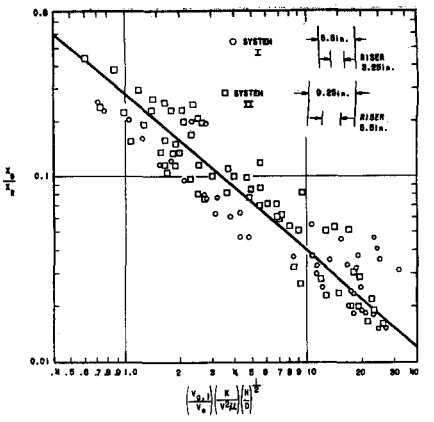

Fig. 13. Correlation of all air-water carry-under data.

of the interface height on the magnitude of the carry under beyond a height of ~ 6 to 8 in. which is reasonably close to $H/D = 1$. This fact is in good agreement with the fluid flow streamline studies discussed previously, which showed similar characteristics. The larger voids in the downcomer than in the riser, as seen in Figure 9, stem from the unique two-phase flow characteristics in downflow. As the downcomer velocity approaches the buoyancy velocity of the gas bubbles, the volume fraction increases sharply since the relative velocity of the two phases is approaching zero. Thus for downcomer flow velocities which are very close to the buoyancy velocity of the gas bubble the downcomer void fractions become very large and, in fact, much larger than riser void fractions.

The effect of temperature is shown in Figure 10. The data shown are for a constant mixture quality and flow rate. The quantity of the gas phase carried under decreases sharply as the temperature is increased. Since all the physical properties of the system remain virtually constant or varied very little, except for the viscosity, it is believed the change in carry under may be attributed to the change in viscosity.

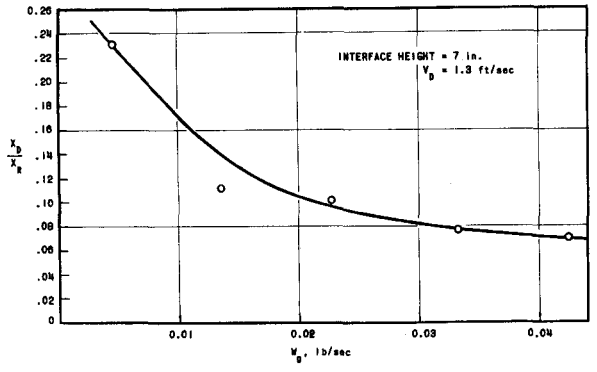

Fig. 12. Weight fraction carry under vs. the riser gas phase flow rate.

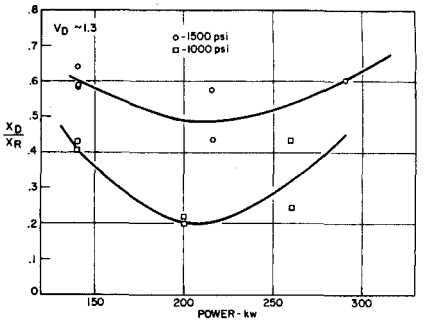

Fig. 14. Weight fraction carry under vs. power input.

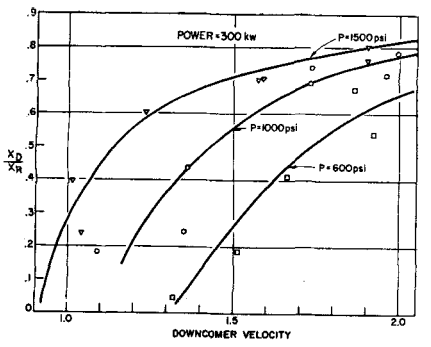

Fig. 15. Weight fraction carry under vs. the downcomer superficial liquid velocity.

A strong effect of the liquid phase mass velocity on carry under is shown in Figure 11. The weight fraction ratio, which is equivalent to the fractional percent carry under, is plotted as a function of the superficial liquid phase downcomer velocity for a fixed gas phase mean velocity and interface height. As can be seen the carry under increases sharply once the velocity threshold has been surpassed and continues to rise steadily but at a lesser rate as the downcomer velocity increases further.

An opposite effect is observed as the gas phase mass velocity is increased as shown in Figure 12. For a constant liquid phase mass velocity and interface height the carry under decreases as the gas phase flow rate is increased. The same behavior pattern was found for each of the liquid mass velocities studied.

The data were correlated according to relationships developed from the analytical study and from dimensional analysis. The dimensionless groupings that were derived from dimensional analysis and found to be relevant are

$$\frac{V_{g,1}}{V_e}, \frac{\sigma}{\mu V}, \frac{gD}{V^2}, \frac{\rho_l}{\rho_g}$$

The data taken on two different systems when plotted according to the following relationship separated

$$\frac{X_D}{X_R} = f\left(\frac{\sigma}{\mu V}\right)\left(\frac{V_{g,1}}{V_e}\right)\left(\frac{gD}{V^2}\right) \quad (31)$$

The separation was found to be due to the diameter factor in the Froude number. It was found that the two sets of data could be brought essentially together by the following relationship

$$\frac{X_D}{X_R} = f\left(\frac{V_{g,1}}{V_e}\right)\left(\frac{1}{V^2\mu}\right)\left(\frac{H}{D}\right)^{1/2} \quad (32)$$

which is identical to Equation (31) with the exception that the D is removed from the Froude number. As a result the relationship is no longer dimensionless. A plot of all the data according to Equation (32) is shown in Figure 13.

The air-water studies demonstrated the dependence of carry under on a number of the system and fluid variables, and therein lies their value. The variables are: system geometry factors such as area ratio between downcomer and riser, diameter of the riser, height of the two-phase mixture interface above the riser; water and air mass velocities and their relative velocities; the temperature dependent physical properties of the fluids such as viscosity, density, surface tension, etc.

High-Pressure Steam-Water Studies

Three series of data were taken at pressures of 600, 1,000, and 1,500 lb./sq. in. The interface height and the vapor liquid mass velocities were varied in a manner similar to that described in the air-water studies.

In general similar trends were developed in a high-pressure data as were observed in the air-water data. The notable exception was the variation of the percentage carry under with increasing gas phase mass flow rate. The air-water data, shown previously in Figure 12, indicated that the carry under decreased as the gas phase mass velocity increased. However the high-pressure data showed a somewhat different trend (see Figure 14). For a fixed pressure and a liquid mass velocity, as the vapor phase flow rate was increased (by increasing power) the carry under initially decreased and reached a minimum and then began to increase. The trend was the same for the three pressures studied. It is possible that with a further increase in the gas mass velocity in the air-water system the carry under would have increased.

The effect of downcomer velocity on carry under for a fixed power and for pressures of 600, 1,000, and 1,500 lb./sq. in. is shown in Figure 15. Again as noted for the air-water data the carry under increases sharply once the velocity threshold has been surpassed and continues to rise steadily but at a lesser rate as the velocity increases. The pressure effect can also be seen in Figure 15. As expected the percent carry under is greater at the higher pressure. The data shown in the previous figures are typical of the large quantity gathered during the study.

Each set of the high-pressure data was adequately correlated by the groupings given in Equation (32), but a family of curves is obtained. The curves separate slightly with pressure, but their slopes are essentially the same. The pressure separation was removed by adding the dimensionless ratio ρ_g/ρ_L as shown in Figure 16. All the high-pressure data for the one geometry are correlated by the following dimensionless groupings:

$$\frac{X_D}{X_R} = f\left(\frac{V_{g,1}}{V_e}\right)\left(\frac{\sigma}{\mu V}\right)\left(\frac{gD}{V^2}\right)^{1/2}\left(\frac{\rho_g}{\rho_L}\right)^{1/2}\left(\frac{H}{D}\right)^{1/2} \quad (33)$$

GENERAL CORRELATION

A correlation encompassing both the air-water and steam-water data was then developed by means of a series of cross plots on the independ-

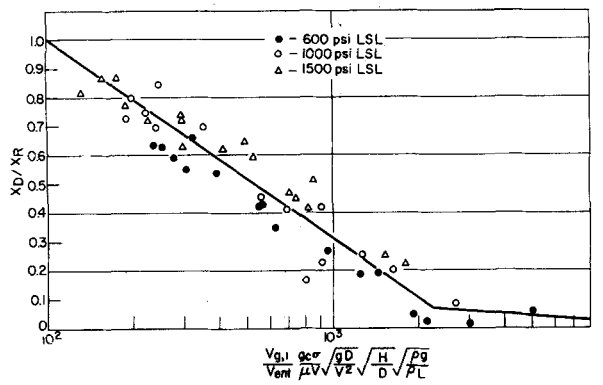

Fig. 16. Correlation of high pressure carry-under data.

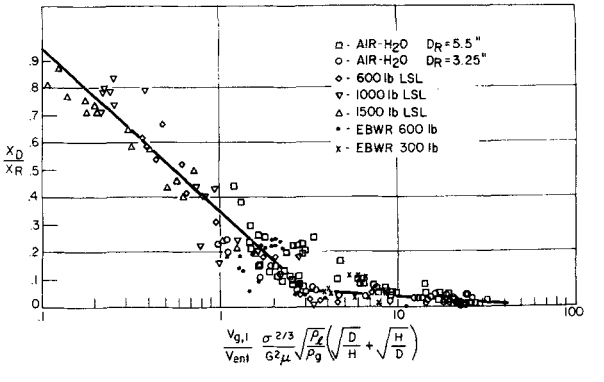

Fig. 17. Correlation of all carry-under data.

ently varied parameters. The nondimensionless correlation adequately accounts for the large majority of the carry-under data, including a few preliminary data points obtained from the EBWR (Experimental Boiling Water Reactor). This correlation is shown in Figure 17. The scatter of the data is not exceptionally bad for such a complex phenomena. The correlation is represented by the following equation:

$$\frac{X_D}{X_R} = -0.04 \log \left[\frac{\left(\frac{V_{g,1}}{V_e}\right)\left(\frac{\sigma^{2/3}}{G^2\mu}\right)\left(\frac{\rho_L}{\rho_g}\right)^{1/2}\left(\sqrt{\frac{D}{H}}+\sqrt{\frac{H}{D}}\right)}{64} \right] \quad (34)$$

In the functional range 3 to 64

$$\frac{X_D}{X_R} = -0.6 \log \left[\frac{\left(\frac{V_{g,1}}{V_e}\right)\left(\frac{\sigma^{2/3}}{G^2\mu}\right)\left(\frac{\rho_L}{\rho_g}\right)^{1/2}\left(\sqrt{\frac{D}{H}}+\sqrt{\frac{H}{D}}\right)}{3.7} \right] \quad (35)$$

for the functional range 0.1 to 3.

It is interesting to note that a rather sharp break point exists suggesting two distinct sets of carry-under conditions. It is postulated that the break point represents the threshold for carry under, and the data points to the right represent that fraction of the vapor flow which is located near the periphery of the riser and which is extremely difficult to separate.

Probably the biggest unknown concerning the correlation is the size factor. The geometry factors in the correlation are given by the term $[(H/D)^{1/2} + (D/H)^{1/2}]$ and indirectly through $V_{g,1}/V_e$ which is a function of the area ratio between the downcomer and the riser. The factor $[(H/D)^{1/2} + (D/H)^{1/2}]$ was arrived at by comparing the preliminary large system reactor data with the small scale loop data. Additional data on larger systems are needed to completely establish the validity of the geometry factors in the correlation.

For carry-under analysis Equations (34) and (35) or Figure 17 can be used in either of several ways. Either the geometry of the system is specified and the expected carry under can be computed, or the required system geometry dimension can be estimated to maintain a specified carry-under level. For a given system the factors ρ_l, ρ_g, σ, and μ are determined by the fluids used and the temperature and pressure of the system. Also the liquid mass velocity is generally established by thermodynamic and hydrodynamic design consideration concerning the heat source.

If it is desired to estimate the percent carry under for a given system, a trial-and-error analysis is required owing to the implicit interrelationship between the downcomer velocity, quality, and void fractions. Interactions between these factors are carried out until convergence is achieved. If it is desired to specify the geometry of the system in order to maintain a carry-under level, the analysis is straightforward and an interative procedure is not required.

It is readily apparent that the prediction of downflow slip ratios becomes an important factor in such an analysis. The accuracy in the downflow slip ratios estimates are reflected strongly in the carry-under analysis. The following relationship is recommended for calculating the downflow slip ratio:

$$\frac{V_g}{V_L} = 0.63 \left(\frac{V^2}{gD}\right)^{0.4} \left[\frac{x}{1-x}\frac{\rho_l}{\rho_g}\right]^{0.2} \quad (36)$$

The correlation was obtained from extensive downflow slip ratio data that was obtained during the course of this study.

The validity of the carry-under correlation presented cannot be specified, primarily owing to the system size factor. Prudent usage of the correlation is therefore advised until further data become available from large systems. The agreement of some preliminary reactor data with the correlation offers promise that it may, in fact, be fairly accurate.

ACKNOWLEDGMENT

This report is the result of an intensive two-year study. During the course of the study a number of people became involved with the research program. Their suggestions, discussions, and contributions aided greatly in bringing the research to a successful conclusion.

Particular recognition need be given to Mr. Peter Zaleski, Prof. Nejat Abyers, Mr. E. A. Spleha, Prof. Bates Chao, Mr. George Lambert, and Mr. Fred Nentwich.

NOTATION

A = area
H = interface height
R = riser radius
D = riser diameter
W = width of downcomer
d = diameter of gas bubble
χ = bubble radius
V = velocity (ft./sec.)
G = liquid mass velocity (lb./sec.-sq. ft.)
α = void volume fraction
X = mixture quality
f = ratio of the circular streamline diameter to the sum of the riser radius and downcomer width
g = gravitational constant
C = drag coefficient
ρ = density (lb./cu. ft.)
σ = surface tension (lb./ft.)
μ = viscosity of liquid (lb./sec.-ft.)

Subscripts

A = annulus
R = riser
D = downcomer
C = sector from which carry under emanates
l = liquid phase
g = gas phase
$L, 1$ = liquid phase in riser
$L, 2$ = liquid in downcomer
$g, 1$ = gas phase in riser
$g, 2$ = gas phase in downcomer
0 = gas bubble
e = entrainment
r = fluid streamline radius
t = tangential
T = true or actual
1 = section of plenum where $\theta = 0$
2 = section of plenum where $\theta = \pi$
3 = section of plenum where $\theta = \pi/2$
c = critical

Superscript

$\rightarrow$ = vector quantity

LITERATURE CITED

1. Allen, H. S., *Phil. Mag.*, **50**, No. 5, pp. 323-338, 519-534 (1900).
2. Pavlushenko, I. S., *J. Appl. Chem. USSR*, **29**, 901 (1956).
3. Miyagi, O., *Technol. Rept. Tohoku Imperial Univ.*, **5**, No. 3 (1925); *Phil. Mag.*, **50**, No. 6, pp. 112-139 (1925).
4. Peebles, F. N., and H. J. Garber, *Chem. Eng. Progr.*, **49**, No. 2, p. 88 (1953).
5. Davies, R. M., and G. Taylor, *Proc. Roy. Soc.*, **A200**, 375 (1950).
6. O'Brien, M., and E. J. Gosline, *Ind. Eng. Chem.*, **27**, 1436 (1935).
7. Rosenberg, B., *Navy Department Report 727* (1950).
8. Waddel, H., *J. Franklin Inst.*, **217**, 459-490 (1934).
9. Petrick, Michael, and B. S. Swanson, *Rev. Sci. Instr.*, **29**, No. 12, pp. 1079-1085 (1958).

Manuscript received July 1, 1962; revision received September 13, 1962; paper accepted October 25, 1962.